Journal of Alloys and Compounds 637 (2015) 443–448

Contents lists available at ScienceDirect

Journal of Alloys and Compounds

journal homepage: www.elsevier.com/locate/jalcom

Superparamagnetic response of zinc ferrite incrusted nanoparticles

K.L. Lopez-Maldonado [a,*], P. de la Presa [b,c], I. Betancourt [d], J.R. Farias Mancilla [a], J.A. Matutes Aquino [e], A. Hernando [b,c], J.T. Elizalde Galindo [a]

[a] Instituto de Ingeniería y Tecnología, Universidad Autónoma de Ciudad Juárez, Av. Del Charro 450 norte, 32310 Ciudad Juárez, Mexico
[b] Instituto de Magnetismo Aplicado (UCM-ADIF-CSIC), PO Box 155, 28230 Las Rozas, Spain
[c] Dpto. Física de Materiales, Univ. Complutense de Madrid, Madrid, Spain
[d] Departamento de Materiales Metálicos y Cerámicos, Instituto de Investigaciones en Materiales, Universidad Nacional Autónoma de México, México, D.F. 04510, Mexico
[e] Centro de Investigación en Materiales Avanzados, Miguel de Cervantes 120, 31109 Chihuahua, Mexico

ARTICLE INFO

Article history:
Received 9 October 2014
Received in revised form 4 February 2015
Accepted 3 March 2015
Available online 9 March 2015

Keywords:
Mechanical alloying
Magnetic properties
Ferrite
Nanocrystals
Microstructure
Langevin model

ABSTRACT

Zinc ferrite is synthesized via mechano-activation, followed by thermal treatment. Spinel $ZnFe_2O_4$ single phase is confirmed by X-ray diffraction. SEM micrographs show large particles with average particle size $\langle D_{part}\rangle$ = 1 μm, with particles in intimate contact. However, TEM micrographs show incrusted nanocrystallites at the particles surface, with average nanocrystallite size calculated as $\langle D_{inc}\rangle \approx 5$ nm. The blocking temperature at 118 K in the ZFC–FC curves indicates the presence of a superparamagnetic response which is attributable to the incrusted nanocrystallites. Moreover, the hysteresis loops show the coexistence of superpara- and paramagnetic responses. The former is observable at the low field region; meanwhile, the second one is responsible of the lack of saturation at high field region. This last behavior is related to a paramagnetic contribution coming from well-ordered crystalline microdomains.

The hysteresis loops are analyzed by means of two different models. The first one is the susceptibility model used to examine separately the para- and superparamagnetic contributions. The fittings with the theoretical model confirm the presence of the above mentioned magnetic contributions. Finally, using the Langevin-based model, the average superparamagnetic diameter $\langle D_{SPM}\rangle$ is calculated. The obtained value $\langle D_{SPM}\rangle$ = 4.7 nm (~5 nm) is consistent with the average nanocrystallite size observed by TEM.

1. Introduction

A continuous and growing interest has been focused on spinel ferrites due to their magnetic properties and unique structure, which makes them useful for technological application [1–4]. These ferrites have $MgAl_2O_4$ crystallographic structure and belong mainly to space group *Fd3m*. In this structure, oxygen conform a FCC structure, with 8 tetrahedral and 16 octahedral sites occupied by the divalent and trivalent transition metal ions. The general formula used to describe spinel ferrites is $(M^{2+}_{1-\delta}Fe^{3+}_{\delta})[M^{2+}_{\delta}Fe^{3+}_{2-\delta}]O_4$. Here M is a transition metal, δ is the inversion parameter (which can range from 0 to 1), round brackets represent the tetrahedral sites (A), and square brackets the octahedral sites [B] [5–7]. Depending on the inversion parameter the spinel can be named as normal ($\delta = 0$), inverse ($\delta = 1$) and, mixed ($0 < \delta < 1$). It is known that inversion degree of ferrites strongly affects their magnetic properties. Commonly, the exchange integrals J_{AB}, J_{BB}, J_{AA} are negative and the antiferromagnetic A–B interaction is stronger that the A–A and B–B interactions; therefore, ferrimagnetism arises from the decompensation of the magnetic moments in the A and B sublattices [2,5].

In the branch of studying the magnetic interactions in ferrites, zinc ferrite represents a very interesting material because Zn is a divalent nonmagnetic cation. In bulk material, the preferred Zn site is tetrahedral (A); and the ferrite orders in the normal spinel structure. As Zn does not have an associated magnetic moment, bulk zinc ferrite is an antiferromagnetic material below T_N = 10.5 K, where weak superexchange interactions between Fe^{3+} cations, located in B-sites, dominate [1,8–10].

However, it has been reported in several works that nanosized zinc ferrite particles produce a ferrimagnetic/superparamagnetic response, which differs markedly from the bulk. This change in the magnetic response is commonly attributed to a cation distribution where some Fe^{3+} ions are forced to move to tetrahedral sites, and consequently, Zn^{2+} migrates to octahedral sites, which alters the long- and short-range magnetic interactions of A and B sites.

* Corresponding author. Tel.: +52 6566884887; fax: +52 6566884813.
E-mail addresses: liliana.lopez.maldonado@gmail.com (K.L. Lopez-Maldonado), pmpresa@ucm.es (P. de la Presa), israelb@unam.mx (I. Betancourt), rurik.farias@uacj.mx (J.R. Farias Mancilla), jose.matutes@cimav.edu.mx (J.A. Matutes Aquino), antonio.hernando@externos.adif.es (A. Hernando), jose.elizalde@uacj.mx (J.T. Elizalde Galindo).

http://dx.doi.org/10.1016/j.jallcom.2015.03.023
0925-8388/

Therefore, the difference in the magnetic response could be attributed to a strong ferrimagnetic coupling due to superexchange interactions between iron ions occupying the A and B sites in the partially inverted spinel structure [2–4,11–14]. Moreover, some researchers report that magnetic properties of zinc ferrites are not only particle size dependent, but they are strongly affected by the synthesis method. For example, conventional ceramic method produces nanoparticles with high magnetization values; whereas, nanoparticles synthesized by co-precipitation method show smaller magnetization values for similar particle sizes [3,9,10,14,15]. Several interesting properties for technological applications may arise from these magnetic variations [16]. Commonly, chemical routes are used to synthesize ferrites; however, mechano-synthesis represents an interesting method because it could induce crystallographic defects that could reinforce the ferrimagnetic responses in zinc ferrites.

In the present work, the magnetic properties of zinc ferrites obtained via mechano-activation are investigated. Due to thermal treatment, nanocrystallites are produced at the surface of highly crystalline microparticles. The contributions of different magnetic responses are analyzed using ZFC/FC curves and hysteresis loops. Superpara- and paramagnetic contributions can be distinguished and analyzed separately by means of susceptibility analysis at the hysteresis loops. Finally, Langevin model is used to investigate the observed superparamagnetic response: nanocrystallite superparamagnetic diameter matches very well with the particle sizes determined by TEM.

2. Experimental procedure

2.1. Synthesis

ZnO and α-Fe_2O_3 powders are used to synthesize zinc ferrite via mechano-activation. First, the precursors are weighted according to stoichiometry to obtain the desired $ZnFe_2O_4$ phase. Then, they are ball-milled during 1 h to mechanically activate the powders, and also to diminish their particle size. The milled powders are pressed into cylindrical pellets of 6 mm of diameter using a pressure of 8 MPa. The pellets are thermally annealed in air at 1373 K during 9 h in order to get the $ZnFe_2O_4$ phase. The sample is cooled down by air quenching. Heat treatment is also used to sinter the sample, and thus ameliorate contacts between particles. Several samples are prepared under same experimental conditions.

2.2. Characterization

Powder samples are obtained by pulverizing the heat treated pellets in an agate mortar and used for some of the characterizations. First, in order to determine the microstructural properties of the samples, they are characterized by X-ray diffraction in a PANalitycal X'PertPro MPD diffractometer, by Scanning Electron Microscopy (SEM) in a field emission microscope JSM7000F, and by transmission electron microscopy (TEM) in a JEOL JEM-220FS microscope. In addition, high resolution TEM images (HRTEM) are obtained to observe nanostructure and crystallinity degree. For transmission electron microscopy characterization, powders of the pulverized sample are dispersed in alcohol and a drop of this is poured in the TEM sample holder. Zero field cooled and field cooled curves (ZFC–FC) are measured in a temperature range from 50 to 300 K with an applied magnetic field of $H = 8 \times 10^3$ A/m by using a Quatum Design VSM magnetometer. Finally, hysteresis loops are measured in the same temperature range, with temperature increments $\Delta T = 25$ K and maximum applied field $H_{max} = 1.6 \times 10^6$ A/m. As milled powders are used for VSM.

3. Theoretical basis

The analysis of magnetic response is carried out by two methods. The first one is the separation of the magnetic susceptibilities; this method is used as a base for the second analysis. The second method is a magnetization model using the Langevin function. This model helps to correlate the structural properties found by SEM/TEM and the magnetic responses observed at the hysteresis loops.

3.1. Hysteresis loops susceptibility analysis

The low field susceptibility, χ_{LF}, is usually calculated from 8×10^3 to 45×10^3 A/m and represents the contribution of all magnetic phases in sample. This can be expressed as follows:

$$\chi_{LF} = \chi_{PM} + \chi_{DM} + \chi_{AFM} + \chi_{FERRI} + \chi_{FERRO} + \chi_{SPM} \quad (1)$$

where PM stands for paramagnetic, DM for diamagnetic, AFM for antiferromagnetic, FERRI for ferrimagnetic, FERRO for ferromagnetic, and SPM for superparamagnetic.

On the other hand, because the ferro- and ferrimagnetic contributions saturate at high fields (HF), only paramagnetic, diamagnetic and antiferromagnetic ordering contribute [17,18]. Therefore, ferri- and ferromagnetic contributions can be discarded at HF, and high field susceptibility can be described as:

$$\chi_{HF} = \chi_{PM} + \chi_{DM} + \chi_{AFM} \quad (2)$$

Consequently, ferri/ferro magnetic contributions can be evaluated by calculating the susceptibility slopes at LF and HF, and subtracting the latter from the former such as:

$$\chi_{FM} = \chi_{LF} - \chi_{HF} \quad (3)$$

Using the previous equations, hysteresis loops that contain more than one magnetic response can be separately analyzed to study the different magnetic contributions [18].

3.2. Magnetization model

Once susceptibility analysis has been carried out, the hysteresis loops are analyzed by means of Langevin model to calculate the magnetization of a system with a particle volume distribution in the superparamagnetic regime [19,20].

The magnetization M of a system of superparamagnetic grains in a magnetic field H is given by

$$M(H,T) = \int_0^\infty \mu L\left(\frac{\mu H}{kT}\right) f(\mu) d\mu \quad (4)$$

where $L\left(\frac{\mu H}{kT}\right)$ is the Langevin function and $f(\mu)$ is the distribution of magnetic moments in a system of superparamagnetic grains. The number of grains per unit volume with magnetic moment between μ and $\mu + d\mu$ is given by $f(\mu)d\mu$.

Then, the saturation magnetization is given by

$$M_S = \int_0^\infty \mu f(\mu) d\mu = N\langle\mu\rangle \quad (5)$$

where $\langle\mu\rangle$ is the mean magnetic moment, and N is the number of grains per unit volume of the sample. On the basis of the M_S value provided by Eq. (5) in terms of the mean magnetic moment $\langle\mu\rangle$ per grain (in units of Bohr magnetons) and the saturation magnetization M_S^{bulk} for bulk $ZnFe_2O_4$ (in units of emu/cm^3) as reference, the average volume $\langle V\rangle$ of the superparamagnetic nanocrystallites can be calculated according to the following ratio

$$V = \frac{M_s}{M_s^{bulk}} \quad (6)$$

Assuming spheroid-like nanocrystallites, the average superparamagnetic diameter $\langle D_{SPM}\rangle$ follows from $\langle D_{SPM}\rangle = 2(3V/4\pi)^{1/3}$.

4. Results

4.1. Microstructural characterization

Fig. 1 shows the XRD pattern for the as sintered sample; all peaks can be easily identified with the $ZnFe_2O_4$ spinel crystalline

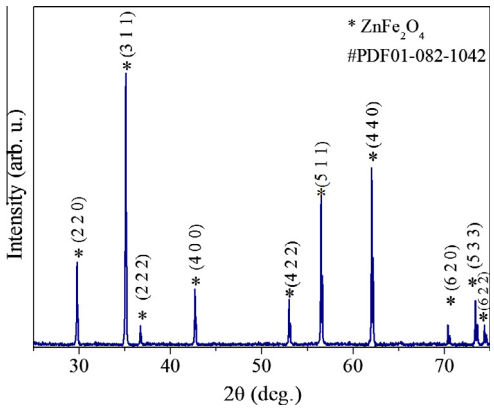

Fig. 1. XRD pattern of the zinc ferrite sintered sample.

phase (#PDF01-082-1042) with the space group $Fd\bar{3}m$. No peaks of any secondary phase are observed. The peaks at the diffraction pattern are tight, which indicates high crystallinity degree and very large crystallite size (>100 nm).

SEM images obtained for the as-sintered pellet show that most of the particles are well adhered to each other (see Fig. 2); although, sample presents some pores and necks that are sintering attributable. Also, average particle size of $\langle D\rangle_{part}$ = 1 μm, with a standard deviation of σ = 0.5 μm, is calculated by measuring more than 100 particles. Fig. 2b shows these large particles observed by TEM.

However, HRTEM micrographs show some nanocrystallites incrusted at the surface of these particles (see Fig. 3). From the images, some planes can be identified; interplanar distances are calculated to be 3 and 4.8 Å, which correspond to the zinc ferrite crystallographic planes (220) and (111), respectively (some planes are indicated at Fig. 3). By means of Digital Micrograph Software, average incrusted crystallite size, $\langle D\rangle_{inc}$, is calculated to be 5 nm with a standard deviation of 2 nm; size distribution can be seen at the inset of Fig. 3. On the basis of the above mentioned structural results, two concepts are defined for this work: (a) *microstructure*, designated for the structure of the larger particles, and (b) *nanostructure*, related to the incrusted crystallites in the large particles.

The reason because no XRD peak broadening was observed due to the nanocrystallites is because the volume fraction of nanocrystallites (<5%) is much lesser than the volume fraction of crystalline microparticles (>95%). This is deduced from HRTEM micrographs which show low density of incrusted nanocrystallites. As XRD characterization has a limit of detection of 5% it would be difficult to observe the broadening of the peaks because of the nanocrystals.

4.2. Zero field cooled – field cooled curves

Magnetic characterization is carried out to study the effects of *micro* and *nanostructures* on the magnetic properties. First, at the ZFC curve (see Fig. 4), a maximum of magnetization at T_B = 118 K is associated with a superparamagnetic blocking temperature (T_B), i.e., the system undergoes from a blocked to an unblocked state where the magnetic susceptibility reaches a maximum. However, as previously detailed, bulk zinc ferrite has an antiferromagnetic response below T_N = 10 K, therefore, a superparamagnetic behavior above T_N is not expected. In this way, some research works indicate that particle size reduction and structural defects promote ferrimagnetic ordering instead of a paramagnetic one [7,11,12,21]. Thus, the maximum at the ZFC curve is associated with a T_B due to a ferrimagnetic contribution that has a Curie temperature above 300 K. Taking into account that *microstructure* has bulk dimensions, a paramagnetic behavior would be expected for the large particles; then, the observed superparamagnetic response should be related to the *nanostructure* of sample. Additionally, an irreversibility point can be observed at T_{irr} = 188 K where ZFC and FC curves split; the difference between T_B and T_{irr} is because of particle size distribution. As reported by other authors, T_B shifts to higher temperatures for larger crystallite/particle sizes [2,4,6,15,20]. Therefore, taking into account that the nanocrystallite size distribution is wide, the smallest nanocrystallites unblock at lower temperatures than the larger ones, generating a broadening of the T_B. In other words, T_{irr} can be defined as the highest value for the T_B of the system [21].

4.3. Hysteresis loops

The hysteresis loops shown in Fig. 5 suggest that both, *micro* and *nanostructures*, contribute in a different way to the magnetic response. First, at HF region, $H > 1.6 \times 10^5$ A/m, the lack of saturation indicates a paramagnetic response. The origin of this paramagnetic behavior can be attributed to *microstructure* which atomic order could be similar to the bulk one. Thus, less structural defects and broken bonds are expected for the largest particles (*microstructure*). Therefore, stoichiometric zinc ferrite with normal spinel structure would generate weak long-range antiferromagnetic order (LRAO) due to superexchange interactions of the irons at the B sub-lattice. This LRAO is destroyed above T_N and paramagnetic response arises [1,2].

In addition to the paramagnetic behavior, a non-linear hysteresis loop at LF region, $H < 1.6 \times 10^5$ A/m, is related to a second magnetic contribution.

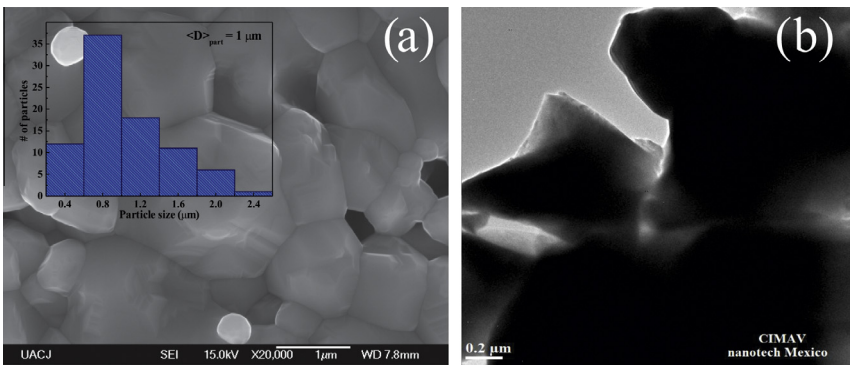

Fig. 2. (a) SEM and (b) TEM micrographs of zinc ferrite sintered sample. At the inset, the calculated particle size distribution.

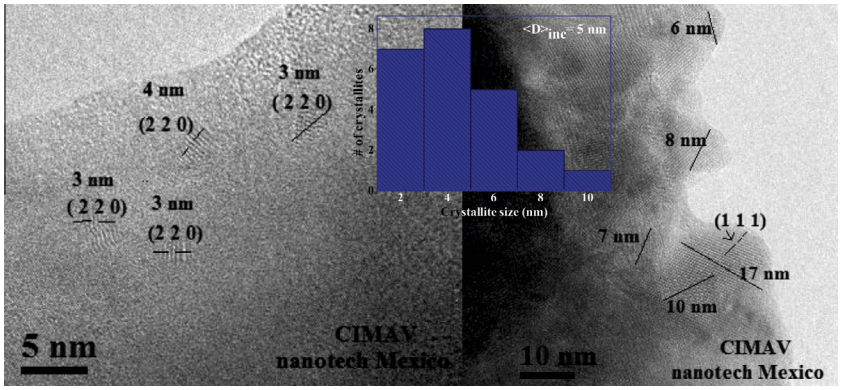

Fig. 3. HRTEM micrographs at the surface of big particles. Nanocrystallite size distribution is shown at the inset graph.

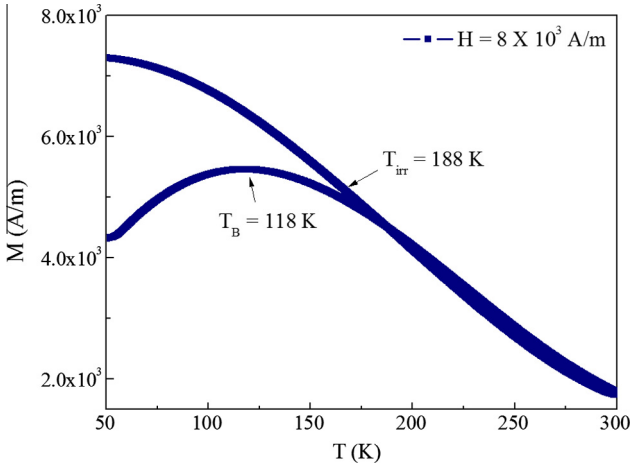

Fig. 4. ZFC and FC curves for the zinc ferrite sample. T_B and T_{irr} temperatures are indicated.

5. Analysis and discussion

Taking into account the hysteresis loops and the observed T_B at the ZFC, the second magnetic contribution is associated with a superparamagnetic response originated by *nanostructure*. Some authors have proposed that, as particle size is reduced to the nanoscale dimensions, zinc ferrite changes from normal to partially inverted spinel. Then, magnetic interactions between Fe^{3+} ions would be enhanced due to the A–B interactions producing a ferrimagnetic alignment. Thus, the observed non-linear hysteresis loop at LF region evidences the presence of ferrimagnetic states with spontaneous magnetization [5,11]. Additionally, the hysteresis loop shape and the ZFC–FC curves indicate that the *nanostructure* is in the superparamagnetic regime above T_B = 118 K.

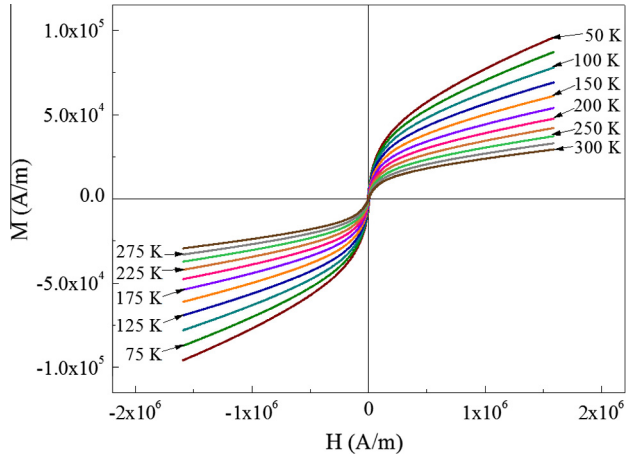

Fig. 5. Hysteresis loops of the as sintered zinc ferrite sample measured at different temperatures. Temperature is indicated with arrows for each curve.

In the following, an attempt to identify the contributions of both structures to the magnetic responses is made by means of the previously described models (Section 3); then, a relationship between magnetic responses and SEM/TEM results is established.

5.1. Model 1: Susceptibility analysis

First, it is necessary to distinguish the magnetic responses coming from *micro* and *nanostructure* in the hysteresis loops (see Section 3.1). In the present work, it is assumed that there are only two magnetic contributions, para- and superparamagnetic associated with the *micro* and *nanostructures*, respectively; any other magnetic contributions are discarded for the sake of clarity.

As explained before, paramagnetic response is the one associated with HF region; therefore, to calculate the paramagnetic susceptibility Eq. (2) is taken as

$$\chi_{HF} = \chi_{PM} \tag{7}$$

Then, superparamagnetic susceptibility, χ_{SPM}, can be calculated by simplifying Eq. (1) as:

$$\chi_{LF} = \chi_{PM} + \chi_{SPM} \tag{8}$$

Therefore, by slope adjustments and calculus, hysteresis loops can be split in these two contributions. Fig. 6 shows both, (a) paramagnetic and (b) superparamagnetic, responses to the (c) total magnetization. As can be seen, linearity of the paramagnetic behavior and saturation of superparamagnetic one confirm the fit goodness, which is calculated from the linear fitting to be adjusted *R*-square ~ 0.99.

Additionally, to prove correct separation of both contributions, two independent fits are carried out on the formerly *separated* superpara- and paramagnetic hysteresis loops:

(i) When a paramagnetic material is studied, the thermal dependence of magnetization should follow Curie law, i.e., magnetization should increase linearly with inverse of temperature [17,18,22]. Therefore, from the *separated* paramagnetic hysteresis loops at all temperatures, *M vs* 1/*T* graphs are obtained for three different magnetic fields, 4×10^5, 8×10^5 and 12×10^5 A/m. Fig. 7a shows the linear

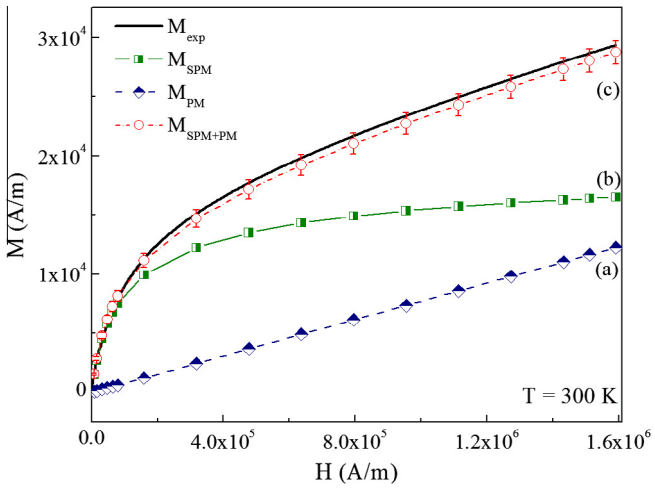

Fig. 6. Magnetization curves and the fittings with theoretical model of (a) paramagnetic response (susceptibility model), (b) superparamagnetic response (magnetization model), and (c) experimental data (black continuous line) and calculated fitted curve: superparamagnetic + paramagnetic responses (red open circles). (For interpretation of the references to colour in this figure legend, the reader is referred to the web version of this article.)

dependence of magnetization with inverse of temperature at the three fields. This linearity proves the correct separation of paramagnetic contribution.

(ii) Further, in the case of non-interacting superparamagnetic nanoparticles, normalized hysteresis loops (M/M_S *vs* H/T) should superpose above blocking temperature [20,22]. As can be seen in TEM micrographs (see Fig. 3), nanocrystallites are well separated to each other by the paramagnetic *microstructure*. Therefore, nanocrystallites can be considered as non-interacting and M/M_S *vs* H/T curves must superpose above T_B. Fig. 7b shows that the normalized hysteresis loops obtained above T_B in fact superpose, corroborating superparamagnetic behavior of the non-interacting nanocrystallites [22–24].

The matching between these two independent fits with theory, confirms that the susceptibility model used to separate the contributions to the hysteresis loops is correct.

The deviation of the normalized hysteresis loops as temperature decreases (shown at the inset of Fig. 7b) is attributed to the particle size distribution and other interactions. It is worth noting that a small ferrimagnetic response may arise due to intrinsic defects and broken bonds. These defects, coming from surface atoms, affect also the first submerged layers, breaking some antiferromagnetic arrange and generating a weak ferrimagnetic behavior. However, superparamagnetic analysis could be made with good accuracy, and the presence of ferrimagnetic response can be neglected in the present work [21].

5.2. Model 2: Langevin-based magnetization model

Finally, Langevin based magnetization model, Eqs. 4–6, is used to calculate the nanocrystallite superparamagnetic diameter, which is related to the magnetic response observed at the hysteresis loops.

Since magnetization is particle size dependent, it is necessary to take into account the relationship between relative magnetization and nanoparticle volume distribution $f(v)$ (Eq. (9)) [19,20,25]. Also, as exposed by Komorida et al. [25] it is first required to establish the relation between magnetic moment distribution to the particle volume distribution, in order to achieve a good fitting of Langevin model to the experimental data.

Thus, the expression used to relate particle volume distribution and magnetization of the system is:

$$\frac{M}{M_S} = \int_0^\infty L\left(\frac{I_S \upsilon H}{kT}\right) f(\upsilon)\, d\upsilon \tag{9}$$

Then, a relationship between magnetic moment and particle volume distribution functions can be deduced by fitting particle volume distribution with a log-normal function. Using this last function, the magnetic moment distribution function can be finally expressed as:

$$f(\mu) = \frac{N}{\mu\sqrt{2\pi}\sigma} \exp\left[-\frac{\ln^2\left(\frac{\mu}{\mu_0}\right)}{2\sigma^2}\right] \tag{10}$$

As shown in other works, this function allows a better fitting of magnetization model (Eqs. (3) and (4)) since it considers the contribution of all particle sizes to the magnetization; this leads to a better understanding of the magnetic properties of the system [19,25].

Eqs. (9) and (10) together with the Langevin-based magnetization model are used to fit the superparamagnetic hysteresis loops. As can be seen in Fig. 6, the magnetization model (red open circles) fits accurately to the experimental data (black continuous line), where the error bars are calculated by using the propagation of

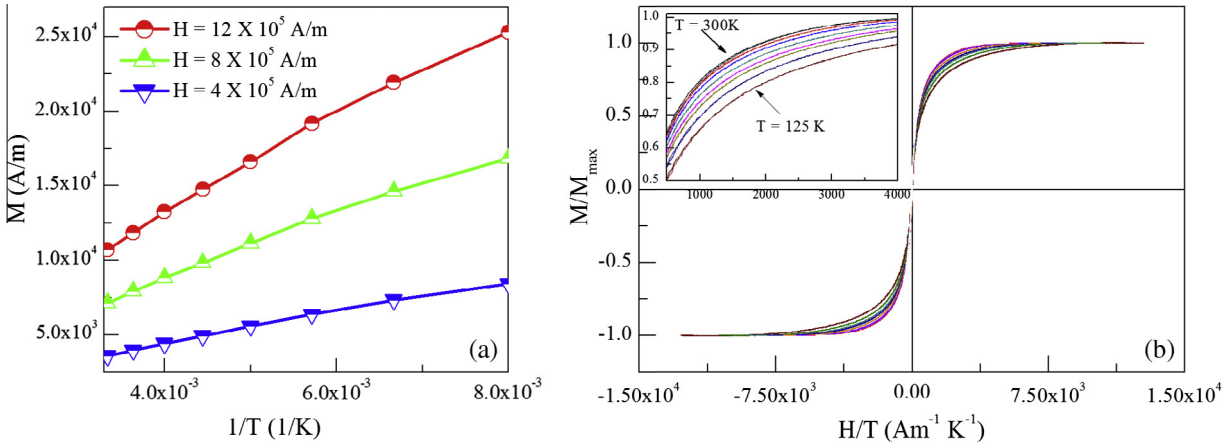

Fig. 7. Fitted curves of: (a) M *vs* $1/T$ for the paramagnetic response, and (b) M/M_S *vs* H/T for the superparamagnetic response. These curves confirms the good splitting of the hysteresis loops using the susceptibility model.

the errors generated by the magnetic measurement and the mass density of the material. From the fitting process and Eq. (5), we obtain an $M_s = 461.66\ \mu_B$. Since $M_s^{bulk} = 90.13$ emu/cm^3 for $ZnFe_2O_4$, we obtain, according to Eq. (6), a volume for the superparamagnetic nanocrystallites of 5.44×10^{-20} cm^3 and hence, a $\langle D_{SPM} \rangle = 4.7$ nm. This size is in excellent agreement with $\langle D \rangle_{inc}$ determined by HRTEM. The magnetic moment calculated for these nanocrystals is about 8 μ_B/unitcell (1 μ_B/formula unit), this value is four times smaller than the magnetic moment per unitcell of magnetite [17,22].

6. Conclusions

$ZnFe_2O_4$ mixed spinel crystalline phase is obtained from mechano-activation. XRD confirms the achievement of zinc ferrite spinel cubic phase. Microstructural characterization shows very crystalline microparticles around 1 μm containing incrusted nanocrystallites at the surface, with average nanocrystallite size $\langle D \rangle_{inc} \approx 5$ nm. From ZFC–FC curves a blocking temperature $T_B = 118$ K and an irreversibility point at $T_{irr} = 188$ K are determined. The difference between T_B and T_{irr} is attributed nanocrystallite size distribution.

The hysteresis loops at different temperatures exhibit at least two contributions, paramagnetic and superparamagnetic behaviors which can be associated with the *micro* and *nanostructures*, respectively. Two magnetic models are used to analyze the observed magnetic contributions: (i) the susceptibility model is used to examine separately the para- and superparamagnetic contributions; (ii) By means of Langevin-based model, the average superparamagnetic diameter $\langle D_{SPM} \rangle$ is calculated. The obtained value $\langle D_{SPM} \rangle = 4.7$ nm is consistent with the average nanocrystallite size observed by TEM.

The different magnetic responses, associated to micro and nanostructure, are related to the size effects on the magnetic properties of zinc ferrite, as it has been reported that size reduction changes the magnetic properties because of a change in the inversion degree of ferrites. Therefore, it can be deduced that the presence of a superparamagnetic behavior indicates that incrusted nanocrystallites play a key role in the magnetic response of the sample.

Acknowledgments

Authors would like to acknowledge to the Universidad Autónoma de Ciudad Juárez, México and Instituto de Magnetismo Aplicado, UCM, Spain for the support given to this research work. This research was supported by UACJ research fund and CONACYT-FOMIX project with Registry No. CHIH-2011-C03-174099.

References

[1] W. Schiessl, W. Potzel, H. Karzel, M. Steiner, G.M. Kalvius, A. Martin, M.K. Krause, I. Halevy, J. Gal, W. Schäfer, G. Will, M. Hillberg, R. Wäppling, Magnetic properties of the $ZnFe_2O_4$ spinel, Phys. Rev. B 53 (1996) 9143–9152.
[2] J.F. Hochepied, P. Bonville, M.P. Pileni, Nonstoichiometric zinc ferrite nanocrystals: syntheses and unusual magnetic properties, J. Phys. Chem. B 104 (2000) 905–912.
[3] J.P. Singh, R.C. Srivastava, H.M. Agrawal, R.P.S. Kushwaha, P. Chand, R. Kumar, EPR study of nanostructured zinc ferrite, Int. J. Nanosci. 07 (2008) 21–27.
[4] C. Yao, Q. Zeng, G.F. Goya, T. Torres, J. Liu, H. Wu, M. Ge, Y. Zeng, Y. Wang, J.Z. Jiang, $ZnFe_2O_4$ nanocrystals: synthesis and magnetic properties, J. Phys. Chem. C 111 (2007) 12274–12278.
[5] H. Yoon, J. Lee, J. Min, J. Wu, Y. Kim, Synthesis, microstructure, and magnetic properties of monosized $Mn_xZn_yFe_{3-x-y}O_4$ ferrite nanocrystals, Nanoscale Res. Lett. 8 (2013) 530.
[6] S.J. Stewart, S.J.A. Figueroa, M.B. Sturla, R.B. Scorzelli, F. García, F.G. Requejo, Magnetic $ZnFe_2O_4$ nanoferrites studied by X-ray magnetic circular dichroism and Mössbauer spectroscopy, Physica B 389 (2007) 155–158.
[7] F. Grasset, N. Labhsetwar, D. Li, D.C. Park, N. Saito, H. Haneda, O. Cador, T. Roisnel, S. Mornet, E. Duguet, J. Portier, J. Etourneau, Synthesis and magnetic characterization of zinc ferrite nanoparticles with different environments: powder, colloidal solution, and zinc ferrite–silica core–shell nanoparticles, Langmuir 18 (2002) 8209–8216.
[8] H. Kavas, A. Baykal, M.S. Toprak, Y. Köseoğlu, M. Sertkol, B. Aktaş, Cation distribution and magnetic properties of Zn doped $NiFe_2O_4$ nanoparticles synthesized by PEG-assisted hydrothermal route, J. Alloys Compd. 479 (2009) 49–55.
[9] S. Nakashima, K. Fujita, K. Tanaka, K. Hirao, T. Yamamoto, I. Tanaka, First-principles XANES simulations of spinel zinc ferrite with a disordered cation distribution, Phys. Rev. B 75 (2007) 174443.
[10] E.J. Choi, Y. Ahn, E.J. Hahn, Size dependence of the magnetic properties in superparamagnetic zinc-ferrite nanoparticles, J. Korean Phys. Soc. 53 (2008) 2090–2094.
[11] S.J. Stewart, S.J.A. Figueroa, J.M. Ramallo López, S.G. Marchetti, J.F. Bengoa, R.J. Prado, F.G. Requejo, Cationic exchange in nanosized $ZnFe_2O_4$ spinel revealed by experimental and simulated near-edge absorption structure, Phys. Rev. B 75 (2007) 073408.
[12] C.N. Chinnasamy, A. Narayanasamy, N. Ponpandian, K. Chattopadhyay, H. Guérault, J.M. Greneche, Magnetic properties of nanostructured ferrimagnetic zinc ferrite, J. Phys.: Condens. Matter 12 (2000) 7795.
[13] C.E. Rodríguez Torres, G.A. Pasquevich, P.M. Zélis, F. Golmar, S.P. Heluani, S.K. Nayak, W.A. Adeagbo, W. Hergert, M. Hoffmann, A. Ernst, P. Esquinazi, S.J. Stewart, Oxygen-vacancy-induced local ferromagnetism as a driving mechanism in enhancing the magnetic response of ferrites, Phys. Rev. B 89 (2014) 104411.
[14] A. Kundu, C. Upadhyay, H.C. Verma, Magnetic properties of a partially inverted zinc ferrite synthesized by a new coprecipitation technique using urea, Phys. Lett. A 311 (2003) 410–415.
[15] L.D. Tung, V. Kolesnichenko, G. Caruntu, D. Caruntu, Y. Remond, V.O. Golub, C.J. O'Connor, L. Spinu, Annealing effects on the magnetic properties of nanocrystalline zinc ferrite, Physica B 319 (2002) 116–121.
[16] K.L. Lopez-Maldonado, L. Vazquez-Zubiate, P. de la Presa, J.A. Matutes-Aquino, J.T. Elizalde-Galindo, Magneto-resistive coefficient enhancement observed around Verwey-like transition on spinel ferrites XFe_2O_4 (X = Mn, Zn), J. Appl. Phys. 115 (2014) 17C705.
[17] B.D. Cullity, C.D. Graham, Introduction to Magnetic Materials, second ed., IEEE Press, John Wiley & Sons, Inc., 2009.
[18] C. Richter, B.A. van der Pluijm, Separation of paramagnetic and ferrimagnetic susceptibilities using low temperature magnetic susceptibilities and comparison with high field methods, Phys. Earth Planet. Inter. 82 (1994) 113–123.
[19] E.F. Ferrari, F.C.S. da Silva, M. Knobel, Influence of the distribution of magnetic moments on the magnetization and magnetoresistance in granular alloys, Phys. Rev. B 56 (1997) 6086–6093.
[20] M. Knobel, W.C. Nunes, L.M. Socolovsky, E. De Biasi, J.M. Vargas, J.C. Denardin, Superparamagnetism and other magnetic features in granular materials: a review on ideal and real systems, J. Nanosci. Nanotechnol. 8 (2008) 2836–2857.
[21] N. Rinaldi-Montes, P. Gorria, D. Martinez-Blanco, A.B. Fuertes, L. Fernandez Barquin, J. Rodriguez Fernandez, I. de Pedro, M.L. Fdez-Gubieda, J. Alonso, L. Olivi, G. Aquilanti, J.A. Blanco, Interplay between microstructure and magnetism in NiO nanoparticles: breakdown of the antiferromagnetic order, Nanoscale 6 (2014) 457–465.
[22] J.M.D. Coey, Magnetism and Magnetic Materials, Cambridge University Press, New York, 2010.
[23] S. Oyarzún, A. Domingues Tavares de Sa, J. Tuaillon-Combes, A. Tamion, A. Hillion, O. Boisron, A. Mosset, M. Pellarin, V. Dupuis, M. Hillenkamp, Giant magnetoresistance in cluster-assembled nanostructures: on the influence of inter-particle interactions, J. Nanopart. Res. 15 (2013) 1–7.
[24] J.I. Levine, Magnetic Materials: Research, Technology and Applications, Nova Science Pub Inc, 2009.
[25] Y. Komorida, M. Mito, H. Deguchi, S. Takagi, T. Tajiri, A. Millán, N.J.O. Silva, M.A. Laguna, F. Palacio, Effects of pressure on maghemite nanoparticles with a core/shell structure, J. Magn. Magn. Mater. 322 (2010) 2117–2126.